Nonlinear modeling of a Free Piston Stirling Engine combined with a Permanent Magnet Linear Synchronous Machine

Mahdi Majidniya, Thierry Boileau, Benjamin Remy, Majid Zandi

Version of Record: https://www.sciencedirect.com/science/article/pii/S135943111933131X
Manuscript_e84bee341aa44787ad16559f296be88f

Nonlinear modeling of a Free Piston Stirling Engine combined with a Permanent Magnet Linear Synchronous Machine

Mahdi MAJIDNIYA[1*], Thierry BOILEAU[1], Benjamin REMY[1], Majid ZANDI[2]

[1]Université de Lorraine, CNRS, LEMTA
F-54000 Nancy, France
[2] Renewable Energies Engineering Department, Shahid Beheshti University
Tehran, Iran
[*](Corresponding author: Mahdi.Majidniya@univ-lorraine.fr)

Abstract - Converting thermal energy to electricity (from renewable or nonrenewable sources) is one of the most required energy conversions around the world. The waste heat of industrial plants and microgrids should also be recovered in the most efficient way. Stirling engines are one of those systems with the highest possible theoretical efficiency and capability of working with different thermal energy sources that have been industrialized. In the following study, a combined model of a β-type Free Piston Stirling Engine (FPSE) and a Permanent Magnet Linear Synchronous Machine (PMLSM) has been proposed. First, both linear and nonlinear equations of the FPSE were extracted and implemented in MATLAB Simulink®. The results were compared and validated with the experimental results. In the second step, an independent model of a standard PMLSM was also implemented in MATLAB Simulink®. At the final step, state equations of the combined system of an FPSE with a PMLSM were developed. These equations were implemented in MATLAB Simulink® and the combined system was controlled. This combined model is a key tool in order to find the optimized control of the combined system (FPSE-PMLSM). This is the main interest of the following study. This system combination will be tested experimentally in future studies.

Keywords: Free Piston Stirling Engine (FPSE), Permanent Magnet Linear Synchronous Machine (PMLSM), System Control, Dynamic simulation, Nonlinear model, Waste heat recovery, Microgrid

Nomenclature

A	Area, m^2
B_v	Friction coefficient
C	Clearance, m
C_f	Darcy friction factor
d	Diameter, m
F	Force, N
i	Current, A
L	Inductance, mH
$M; m$	Mass, kg
P	Pressure, Pa - Power, kW
R	Gas constant, J/kgK - Resistance, Ω
Re	Reynolds number
T	Temperature, K

Greek symbols

γ	Specific heat ratio
$\theta; \phi$	Angle
ρ	Density, kg/m3
ψ_f	Flux linkage, Wb
ω	Frequency, rad/s

Index and exponent

$b; B$	Buffer
c	Compression
$d; D$	Displacer
$d; q$	Axis
e	Expansion
el	Electric

$u; U$	Velocity, m/s	em	Electromagnetic
v	Voltage, V	h	Heater
V	Volume, m^3	k	Cooler
X	Maximum amplitude, m	m	Mover
x	Displacement, m	p	Power piston
$\dot{x}$	Velocity, m/s	r	Regenerator
$\ddot{x}$	Acceleration, m/s^2	w	Wire

1. Introduction

Due to increase in energy demand, a lot of methods were developed to produce it. In most of these methods, a heat source is converted into electricity. This kind of conversion can be divided into two categories: 1- nonrenewable power plants extracting energy from fossil fuels or nuclear fission; 2- renewable power plants such as geothermal or solar power plants. In all these power plants, efficiency and price play a vital role. To increase efficiency, a solution is to recover energy from waste heat of all kind of power plants. One way to aim this goal is to use a Stirling engine.

Stirling engine was invented by R. Stirling in 1816 [1]. Due to their external combustion, these systems can work with variable energy sources such as biomass [2], solar energy [3], natural gas or gasoline [4,5]. From transmission mechanism point of view, Stirling engines can be classified into two types: kinematic ones and dynamic ones [6,7]. In kinematic Stirling engines, power piston and displacer are synchronized by a rigid connection. In dynamic ones, power piston and displacer are synchronized by their dynamic behavior. The Free Piston Stirling Engine (FPSE) is a dynamic one. FPSE was invented by W.T. Beale in 1964 and patented in 1971 [8].

An FPSE combined with a linear alternator can work with variable heat sources and compression ratios. This system has higher efficiency cost ratio than the traditional power generators [9]. Also, due to elimination of crank-shaft, it's a more compact, lightweight system [9] and better sealed to keep gasses like Helium or Hydrogen inside it for more working cycles [10]. This system has a high level of reliability that it can work in hard conditions such as a Lunar base [11].

All these aspects make FPSE-linear alternator combined system an essential topic to study. Most of these studies analyzed the combined system by only focusing on one part of it and did not study the whole system in detail. To have more realistic system behavior and develop a more efficient control method to improve its efficiency and stability, it is necessary to study thermodynamic, mechanic and electric behavior of the system at the same time with fine models.

Studies that focused on analyzing a linear alternator for FPSE and did not model it in detail are a large part of such studies. Kim et al. [12] theoretically and experimentally designed and studied a linear oscillatory single-phase permanent magnet generator that can be used with an FPSE. They analyzed different types of linear generator to find the suitable one for FPSE. Their focus was on linear generator and they didn't present a model for FPSE. Zheng et al. [13] also by defining two simple equations to calculate the force and the power of the FPSE and presenting a linear model for a three phase Permanent Magnet Linear Synchronous Machine (PMLSM), studied the control strategies that can be applied during starting and generating

modes. They also studied their control methods experimentally. In the experimental setup, due to limitations, they used a brushless DC motor as a prime mover engine to simulate FPSE and convert rotary motion to linear one by using a crankshaft mechanism. Dang et al. [14–16] theoretically and experimentally in three different papers studied and optimized a tubular linear induction generator to be used with FPSE. They didn't propose a model for FPSE and only focused on generator system. Hew et al. [17] without presenting a model for FPSE or linear generator, experimentally studied a 5 kW linear generator to be used in FPSE. Among all the suggested linear alternators, between permanent magnet ones and induction ones, due to higher efficiency of permanent magnet linear alternator [15], this system was chosen for the present study. Moreover, between three phase and single phase permanent magnet alternators, the three phase ones are more economical and need less wire compared to the equivalent single phase ones [18].So, for the present study a three phase permanent magnet linear synchronous machine was chosen.

Beside the previous studies that focused on the linear alternator, some studies did not model it in detail and just presented it as a damper next to the FPSE. Boucher et al. [19] analytically studied a linear model of a dual FPSE combined with a PMLSM that modeled as a damper. Karabulut et al. [20] also proposed and analyzed thermal and dynamic behavior of a Martini type FPSE with a linear model. In their model they identified alternator as a damper for FPSE and didn't analyze it in detail.

Furthermore, some studies presented a linear model of a combined FPSE-linear alternator system. Zheng et al. [21] in continuation of their previous study [13] presented a combined system of an FPSE with a 1 kW PMLSM. In their study, they presented a linear model for FPSE. For the experimental setup, due to the limitations, they used a brushless DC motor combined with a crankshaft mechanism to model FPSE. Zhu et al. [22] used thermoacoustic theory to develop a linear model of a micro-CHP system consisting of a β-type FPSE acoustically coupled with a linear alternator. They also built an experimental setup to validate their theoretical model. In all these studies, even studies that analyzed both FPSE and PMLSM in detail, they used a linear model for FPSE.

Only a few studies of a combined FPSE-linear alternator system have been done, and all have been on simplified systems, so a comprehensive analysis of such a system seems necessary. According to the best knowledge of the authors, considering the combination of an FPSE with a PMLSM regarding the nonlinear equations of FPSE has not been done before. Using nonlinear equations of FPSE makes the system more realistic and possible to study the instabilities of the FPSE in such combination. In addition, as it will be shown in the following sections the linear model of FPSE, from authors point of view, is not the most reliable model to study the system in all operating conditions.

In this study, a combined system of an FPSE model and a PMLSM is investigated. First, FPSE was modeled and its nonlinear equations were solved in MATLAB Simulink®. Also, a linear model of the FPSE was simulated in MATLAB® in order to identify the model that can have the best prediction of the real system behavior. After validating FPSE model with available experimental results, PMLSM was modeled and controlled with three controllers (two current controllers and one speed controller) in MATLAB Simulink®. To combine these systems, their equations were joined, solved and the combined system was controlled in MATLAB Simulink®. Controlling such system makes it possible to avoid conditions leading to FPSE instability. Moreover, it is feasible to control the system in all transient operating modes to get the best performance. This study is a foundation for the experimental one that will be done in a close future.

2. System Description

In Figure 1 schematic of the combined FPSE-PMLSM system is shown. As it can be seen, power piston is connected to the PMLSM mover with a rigid rod. There are two current sensors to measure the currents (i_a and i_b), and one position sensor to measure the mover position (x). These measures are used to control the system with DSP. There are three controllers, two of them dedicated to the currents and one dedicated to the speed. Due to star connection between the windings, equation: $i_a + i_b + i_c = 0$ can be applied. Thus, the third current can be calculated based on the other two currents.

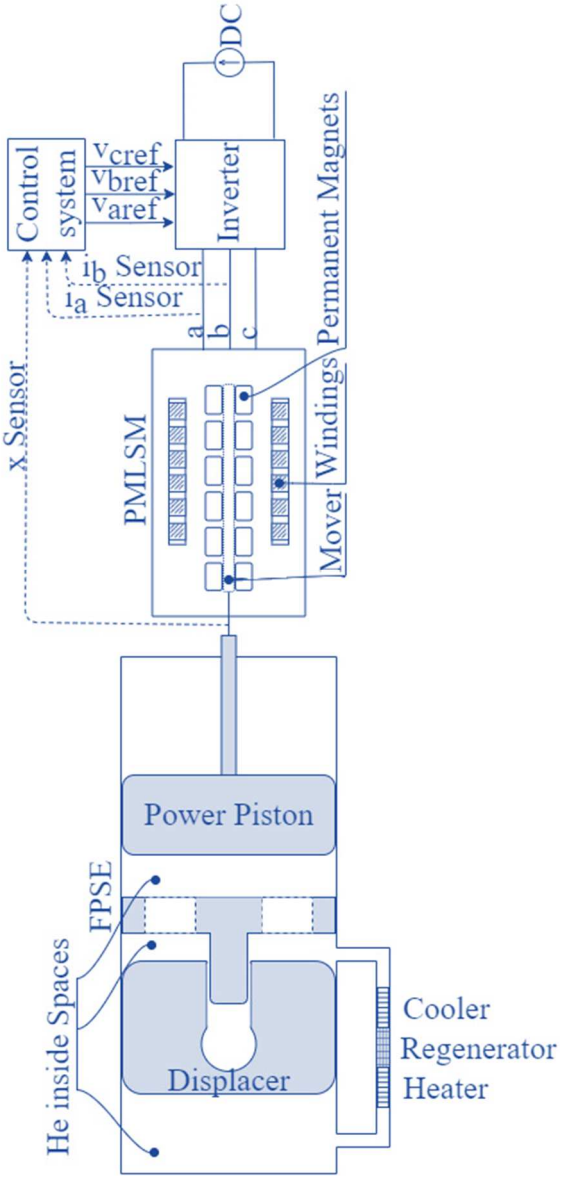

Figure 1: FPSE-PMLSM schematic

3. FPSE Analysis

The modeled FPSE is based on Sunpower RE-1000 engine. A simple schematic of such system is shown in Figure 2.

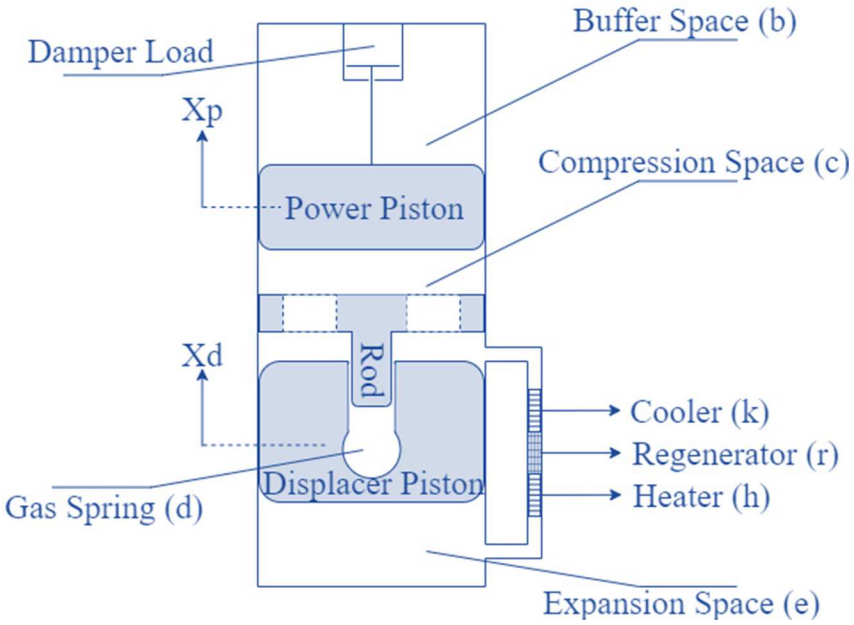

Figure 2: FPSE schematic

As it can be seen, the main spaces inside an FPSE are buffer space (b subscript), compression space (c subscript), displacer gas spring space (d subscript), expansion space (e subscript), heater space (h subscript), cooler space (k subscript) and regenerator space (r subscript). It is assumed that there is no leakage and the total mass of the gas inside the system is constant, so equation (1) can be written as:

$$M = m_c + m_e + m_h + m_k + m_r \tag{1}$$

By assuming the isothermal conditions and applying ideal gas law, equation (1) can be rewritten as:

$$M = \frac{P}{R}\left(\frac{V_c}{T_k} + \frac{V_e}{T_h} + \frac{V_h}{T_h} + \frac{V_k}{T_k} + \frac{V_r}{T_r}\right) \tag{2}$$

For the purposes of calculating mass, the pressure throughout the system is assumed to be constant. Cooling, heating, and regenerator volumes are constant, but compression and expansion volumes are variable that can be calculated at each moment based on equations (3) and (4):

$$V_c = A_p\left(x_p + C_c\right) - (A_d - A_{rod})x_d \tag{3}$$

$$V_e = A_d(x_d + C_e) \tag{4}$$

C_c and C_e are compression and expansion spaces clearance (constant), respectively. Also, the regenerator temperature can be calculated as [23]:

$$T_r = \frac{T_h - T_k}{ln(T_h/T_k)} \tag{5}$$

By putting equations (2) -(5) in equation (1) and doing some simplifications, equation (6) will be obtained:

$$P = \frac{MR}{V_{avT}}\left(1 + \frac{A_p x_p - (A_d - A_{rod})x_d}{T_k V_{avT}} + \frac{A_d x_d}{T_h V_{avT}}\right)^{-1} \tag{6}$$

$$V_{avT} = \frac{A_p C_c}{T_k} + \frac{A_d C_e}{T_h} + \frac{V_h}{T_h} + \frac{V_k}{T_k} + \frac{V_r}{T_r} \tag{7}$$

Here, the parameter $\frac{MR}{V_{avT}}$ can be defined as mean pressure (P_{mean}).

Based on Figure 2, by writing the force balance around the power piston (p Subscript) and the displacer piston (d Subscript), following dynamic equations will be obtained [23]:

$$m_p \ddot{x}_p = A_p(P_c - P_b) - F_{load} \tag{8}$$

$$m_d \ddot{x}_d = A_d P_e - (A_d - A_{rod})P_c - A_{rod}(P_d) = A_d(P_e - P_c) + A_{rod}(P_c - P_d) \tag{9}$$

The pressure difference between expansion and compression spaces can be calculated based on the pressure drop between these spaces that is shown in equation (10):

$$P_e - P_c = \Delta P \tag{10}$$

The pressure drop will be calculated in section 3.1. It is possible to assume that the compression space pressure (P_c) is equal to the instantaneous system pressure (P). Also, by assuming adiabatic conditions in buffer and displacer gas spring spaces and having perfect gas, the buffer and displacer gas spring pressures can be calculated by equation (11) and (12), respectively [23]:

$$P_b = P_{mean}\left(\frac{V_B}{V_b}\right)^{\gamma} \tag{11}$$

$$P_d = P_{mean}\left(\frac{V_D}{V_d}\right)^{\gamma} \tag{12}$$

γ is specific heat ratio of the gas. V_B and V_D are average volumes and V_b and V_d are instantaneous volumes for buffer and displacer gas spring spaces, respectively. The instantaneous volumes can be calculated as [23]:

$$V_b = V_B - A_p x_p \tag{13}$$

$$V_d = V_D - A_{rod} x_d \tag{14}$$

By putting equations (13) and (14) in equations (11) and (12), respectively and then combining equations (6) -(12), the final nonlinear set of dynamic equations that are used to model the FPSE will be achieved:

$$m_p \ddot{x}_p = A_p P_{mean}\left(\left(1 + \frac{A_p x_p - (A_d - A_{rod})x_d}{T_k V_{avT}} + \frac{A_d x_d}{T_h V_{avT}}\right)^{-1} - \left(\frac{V_B}{V_B - A_p x_p}\right)^{\gamma}\right) - F_{load} \tag{15}$$

$$m_d \ddot{x}_d = A_d \Delta P + A_{rod} P_{mean}\left(\left(1 + \frac{A_p x_p - (A_d - A_{rod})x_d}{T_k V_{avT}} + \frac{A_d x_d}{T_h V_{avT}}\right)^{-1} - \left(\frac{V_D}{V_D - A_{rod} x_d}\right)^{\gamma}\right) \tag{16}$$

3.1. Pressure Drop

To calculate the pressure drop, general form of the pressure drop equation is used [23]:

$$\Delta P = \frac{1}{2}\rho\left(\frac{C_f L}{d_h}\right)u|u| \tag{17}$$

C_f is Darcy friction factor, ρ is gas density, u is instantaneous velocity of the gas, and L and d_h are length and hydraulic diameter of the component, respectively. The total pressure drop is the summation of the pressure drops in heater, cooler and regenerator. The heater and cooler constructed from homogeneous bundles of smooth circular pipes and regenerator consists of stacked wire meshes. To calculate instantaneous velocity, volumetric flow rate through heat exchangers can be calculated based on the equations (3) and (4) as equation (18) [23]:

$$\dot{V} = \dot{V}_c - \dot{V}_e = A_p \dot{x}_p - (2A_d - A_{rod})\dot{x}_d \tag{18}$$

Then instantaneous velocity for each heat exchanger can be approximately calculated as:

$$u_i = \frac{\dot{V}}{A_i} \; ; i = k; h; r \tag{19}$$

General definition of hydraulic diameter is:

$$d_H = \frac{4V}{A_w} \tag{20}$$

V is the total volume and A_w is the wetted area. For the porous material in the regenerator, the hydraulic diameter is defined in equation (21) [23]:

$$d_H = \frac{d_w \times Porosity}{1 - Porosity} \tag{21}$$

d_w is the wire mesh diameter. The Darcy friction factor for heater, cooler and regenerator are presented in Table 1.

For heater and cooler:	$Re < 2000$	$C_f = 64/Re$
	$Re > 2000$	$C_f = 0.316Re^{-0.25}$
For regenerator:	$Re < 60$	$C_f = 4 \times 10^{(1.73 - 0.93 \log Re)}$
	$60 < Re < 1000$	$C_f = 4 \times 10^{(0.714 - 0.365 \log Re)}$
	$Re > 1000$	$C_f = 4 \times 10^{(0.015 - 0.125 \log Re)}$

Table 1: Darcy friction factor [24,25]

For Reynolds calculation, peak speed values (equation (22)) of heat exchangers were used. By using equation (18) and assuming sinusoidal displacement, it is possible to calculate the maximum amplitude of volumetric flow rate. Then based on equation (19) the maximum speed values can be calculated as equation (22) [23]:

$$U_{\max(i)} = \frac{\omega\sqrt{\left(A_p X_p\right)^2 + \left((2A_d - A_{rod})X_d\right)^2 - 2A_p X_p (2A_d - A_{rod}) X_d \sin\phi}}{A_i} \; ; i = k; h; r \tag{22}$$

X_p and X_d are maximum displacement amplitude of power piston and displacer piston, respectively. ϕ is the phase shift between power piston and displacer piston movement.

Now, based on the all the equations, the block diagram of the FPSE in MATLAB Simulink® is shown in Figure 3.

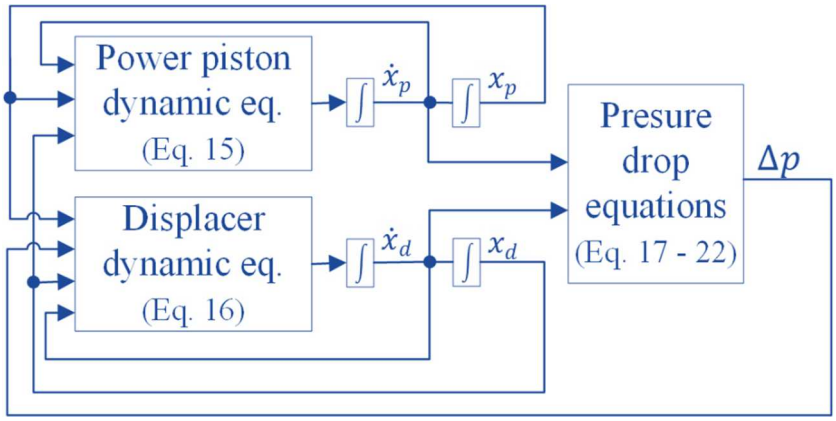

Figure 3: Block Diagram of FPSE

3.2. Linearized Equation

According to Urieli and Berchowitz [23], FPSE equations can be linearized so that they can be solved simply. The linearization process was done for the whole set of equations and the simplified equations are:

$$\ddot{x}_p = K_{pp}x_p + K_{pd}x_d + D_{pp}\dot{x}_p + D_{pd}\dot{x}_d \tag{23}$$

$$\ddot{x}_d = K_{dp}x_p + K_{dd}x_d + D_{dp}\dot{x}_p + D_{dd}\dot{x}_d \tag{24}$$

$$K_{pp} = \frac{A_p^2}{m_p} P_{mean}\left(\frac{1}{T_k V_{avT}} + \frac{\gamma}{V_B}\right) \tag{25}$$

$$K_{pd} = -\frac{A_p^2}{m_p V_{avT}} P_{mean}\left(\frac{1}{T_h} - \frac{\left(1 - A_{rod}/A_p\right)}{T_k}\right) \tag{26}$$

$$D_{pp} = -\frac{\left(C_{damp} + C_{H_b}\right)}{m_p} \tag{27}$$

$$D_{pd} = 0 \tag{28}$$

$$K_{dp} = -\frac{A_p A_{rod} P_{mean}}{m_d T_k V_{avT}} \tag{29}$$

$$K_{dd} = -\frac{A_{rod}}{m_d} p_{mean}\left(\frac{A_p}{T_h V_{avT}} - \frac{\left(A_p - A_{rod}\right)}{T_k V_{avT}} + \frac{\gamma A_{rod}}{V_D}\right) \tag{30}$$

$$D_{dp} = C_p/m_d \tag{31}$$

$$D_{dd} = \left(C_d - C_{H_d}\right)/m_d \tag{32}$$

C_{H_b} and C_{H_d} are buffer and displacer gas spring damping coefficients, respectively. C_{damp} is load damping coefficient and C_p and C_d can be calculated based on linearized pressure drop equation as [23] :

$$A_d \Delta p = C_p \dot{x}_p + C_d \dot{x}_d \tag{33}$$

C_{H_b},C_{H_d},C_p and C_d can be calculated based on [23]. Linear equations were solved in MATLAB® with ode45 solver.

3.3. Linear and nonlinear model comparison

In this section, the linear and nonlinear equations will be compared.

As it can be seen in equations (15) and (16) there are four important terms that should be linearized to obtain the linear set of equations ((23) and (24)). Three of these terms are pressures (equations (6), (11) and (12)) and the forth one is pressure drop (equation (17)). Equations (6), (11) and (12) can be linearized by using Taylor series. These equations after and before linearization were compared and the results are in good accordance. For equation (17) the method of linearization is different. Based on the common linearization method [23] to linearize equation (17), it is necessary to find an equivalent linear damper that dissipates the same energy as pressure drop dissipates. To simplify the calculation of energy dissipation from equation (17), it is assumed that the flow velocity can be approximated by [23]:

$$u = U_{\max} \cos \omega t \tag{34}$$

Based on this assumption, the linearized pressure drop based on [23] will be as:

$$\Delta P \cong \frac{4\rho}{3\pi}\left(\frac{C_f L}{d_h}\right) U_{\max} u \tag{35}$$

Based on the assumption of equation (34) for the flow velocity, the results of linearized pressure drop (35) and nonlinear pressure drop (17) are close.

For the FPSE RE-1000 defined with the parameters given in table 2, after solving equations (15) and (16) in Simulink®, the flow velocity is calculated from equations (18) and (19) instead of equation (34). The results of the linear and nonlinear pressure drop for the FPSE RE-1000 are given in Figure 4.

T_h	814.3 K	d_w	0.00889 cm	V_D	37.97 cm^3
T_k	322.8 K	L_k	7.92 cm	V_r	56.37 cm^3
P_{mean}	71 bars	L_h	18.34 cm	A_{w_k}	115.2 cm^2
$Porosity$	75.9 %	L_r	6.44 cm	X_p	1.145 cm
m_d	0.426 kg	A_h	1.4898 cm^2	X_d	1.233 cm
m_p	6.2 kg	A_k	2.6163 cm^2	Load damping	580 Ns m^{-1}
d_p	5.718 cm	A_r	8.745 cm^2	ϕ	-42.5°
d_d	5.67 cm	C_c	1.83 cm	ω	2π ×30 rad/s
d_{rod}	1.663 cm	C_e	1.861 cm	Gas	He
d_h	0.2362 cm	V_B	2615 cm^3		

Table 2: Input parameters of FPSE [23]

In Table 2 d_i and L_i are diameter and length of component i, respectively and V_i defines volume.

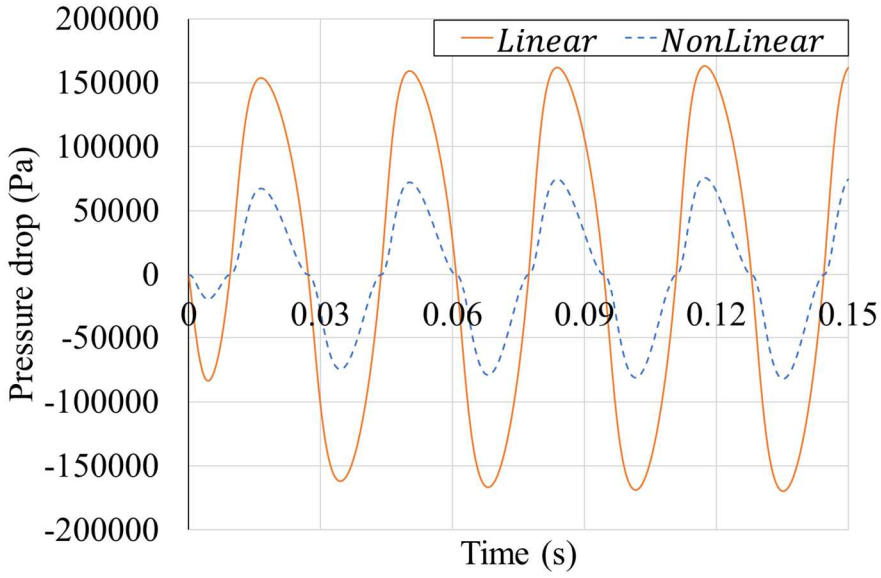

Figure 4: Linear and nonlinear pressure drop

As can be seen there is large difference between the linear and the non-linear model for pressure drop. The effects of these differences on the system response are shown in Figure 5.

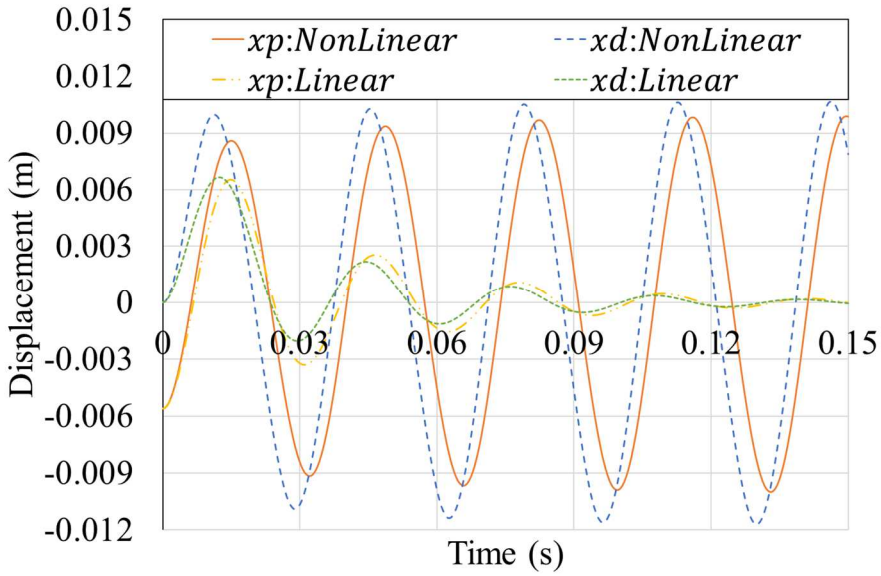

Figure 5: Results of linear and nonlinear FPSE modelling

As it is shown in Figure 5 linear model does not have a steady behavior and cannot identify the realistic behavior of the system for the present case. On the other hand, Nonlinear model after a few cycle becomes stable and shows steady behavior. Thus, nonlinear model of the system will be used.

3.4. FPSE Model Validation

The results of the nonlinear model based on the input data of Table 2 are compared to the experimental results obtained from the FPSE RE-1000[23] in Table 3.

	Frequency (Hz)	Phase Angle (°)	Amplitude Ratio (Xd/Xp)	Output Power (kW)

Exp. Results [23]	30	-42.5	1.06	1.00
Nonlinear Model	29.8	-32.97	1.1239	1.015
Error	0.67%	22.4%	-6%	-1.5%

Table 3: FPSE validation

In Table 3, frequency identifies the piston movement frequency and phase angle identifies the phase shift between piston and displacer movement. As it can be seen in Table 3 there is a good consistency between nonlinear model and experimental results. Thus, the nonlinear model can be used for the combine system simulation.

4. PMLSM Analysis

In this section mathematical model of the PMLSM will be described. First, due to hard control of the PMLSM in three phase ($a-b-c$) frame directly, usually equations are written in dual phase ($d-q$) frame. To convert $a-b-c$ frame to $d-q$ frame and vice versa, Park and Concordia transformations are used [26]. By using these transformations three-phase time-domain signals from a stationary phase coordinate system ($a-b-c$) will convert to a rotating coordinate system ($d-q$) [26]:

$$\begin{bmatrix} Y_\alpha \\ Y_\beta \end{bmatrix} = \sqrt{\frac{2}{3}} \begin{bmatrix} 1 & -1/2 & -1/2 \\ 0 & \sqrt{3}/2 & -\sqrt{3}/2 \end{bmatrix} \begin{bmatrix} Y_a \\ Y_b \\ Y_c \end{bmatrix} \tag{36}$$

$$\begin{bmatrix} Y_d \\ Y_q \end{bmatrix} = \begin{bmatrix} \cos\theta & \sin\theta \\ -\sin\theta & \cos\theta \end{bmatrix} \begin{bmatrix} Y_\alpha \\ Y_\beta \end{bmatrix} \tag{37}$$

$$\begin{bmatrix} Y_\alpha \\ Y_\beta \end{bmatrix} = \begin{bmatrix} \cos\theta & -\sin\theta \\ \sin\theta & \cos\theta \end{bmatrix} \begin{bmatrix} Y_d \\ Y_q \end{bmatrix} \tag{38}$$

$$\begin{bmatrix} Y_a \\ Y_b \\ Y_c \end{bmatrix} = \sqrt{\frac{2}{3}} \begin{bmatrix} 1 & 0 \\ -1/2 & \sqrt{3}/2 \\ -1/2 & -\sqrt{3}/2 \end{bmatrix} \begin{bmatrix} Y_\alpha \\ Y_\beta \end{bmatrix} \tag{39}$$

Y can be current (i) or voltage (v). θ can be calculated based on equation (40):

$$\theta = \int \frac{\pi}{\tau} \dot{x}\, dt \tag{40}$$

τ is pole pitch and $\dot{x}$ is the PMLSM mover speed. Based on these transformations, PMLSM system equations in $d-q$ frame will be as [26]:

$$v_d = L_d \frac{di_d}{dt} + Ri_d - \frac{\pi}{\tau} \dot{x} L_q i_q \tag{41}$$

$$v_q = L_q \frac{di_q}{dt} + Ri_q + \frac{\pi}{\tau} \dot{x} \left(L_d i_d + \sqrt{3/2}\, \psi_f \right) \tag{42}$$

$$F_{em} = \frac{\pi}{\tau} \left(\sqrt{3/2}\, \psi_f i_q + \left(L_d - L_q \right) i_d i_q \right) \tag{43}$$

$$m_m \ddot{x} = F_{em} - B_v \dot{x} - F_{load} \tag{44}$$

$$P_{em} = F_{em} \dot{x} \tag{45}$$

$$P_{el} = v_q i_q + v_d i_d \tag{46}$$

L_d and L_q are $d-q$ axis inductances, R is winding resistance, ψ_f is maximum permanent magnet flux linkage, m_m is PMLSM mover mass, B_v is friction coefficient, F_{em} and P_{em} are electromagnetic force and power, respectively and P_{el} is electric power.

Block diagram of the PMLSM is shown in Figure 6. This block diagram has 3 sections: 1- PMLSM model, 2- Inverter and 3- Control system. Also, two reference input values that were used to drive the system model are shown in Figure 6. The i_d reference is equal to zero and $\dot{x}$ reference is a sinusoidal wave.

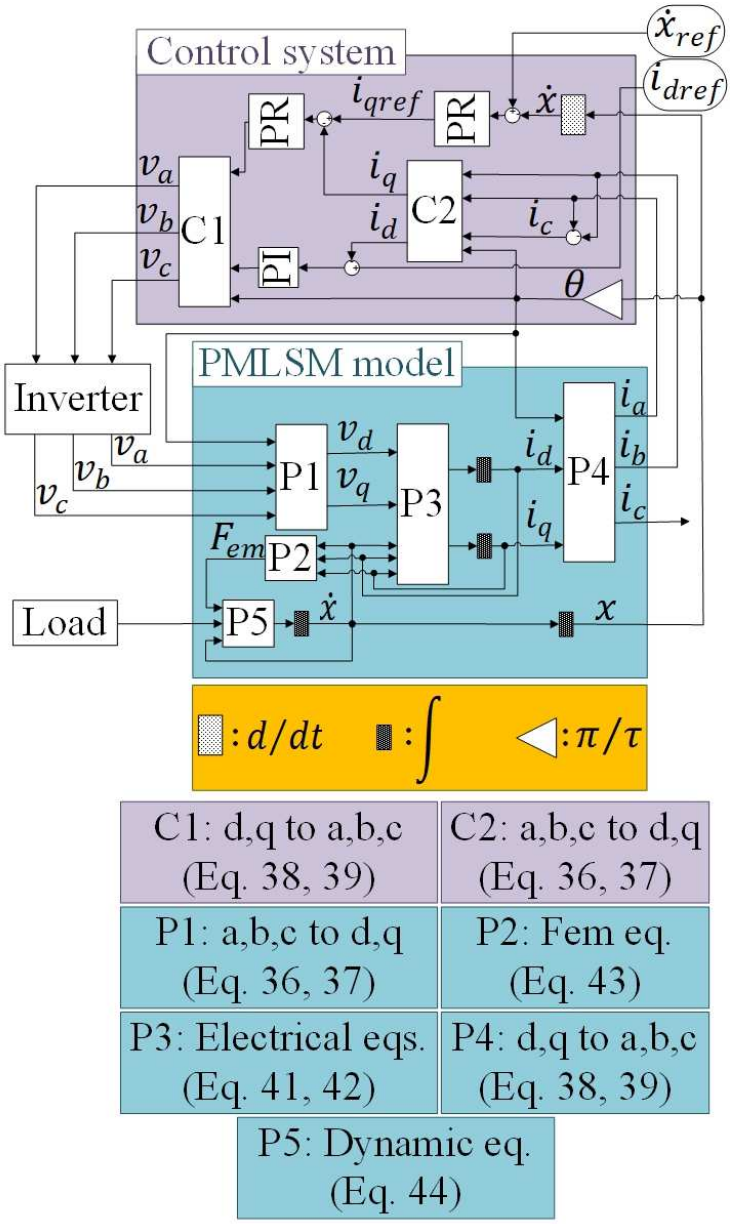

Figure 6: Block diagram of PMLSM

As it can be seen, one PI (Proportional Integrator) and two PR (Proportional Resonant) controllers were used to control the PMLSM system. Two of these controllers are controlling the currents and another one is controlling the velocity.

It should be noted that in order to have a more realistic system, an inverter which is based on a classical PWM was also simulated.

4.1. PMLSM Control

The simulation results of the PMLSM model based on the data of Table 4 are shown in Figure 7 and Figure 8.

R	0.448 (Ω)	L_q	3.01 (mH)	B_v	10
L_d	1.77 (mH)	ψ_f	0.0513 (Wb)	m_m	0.824 (kg)

Table 4: Input parameters of PMLSM

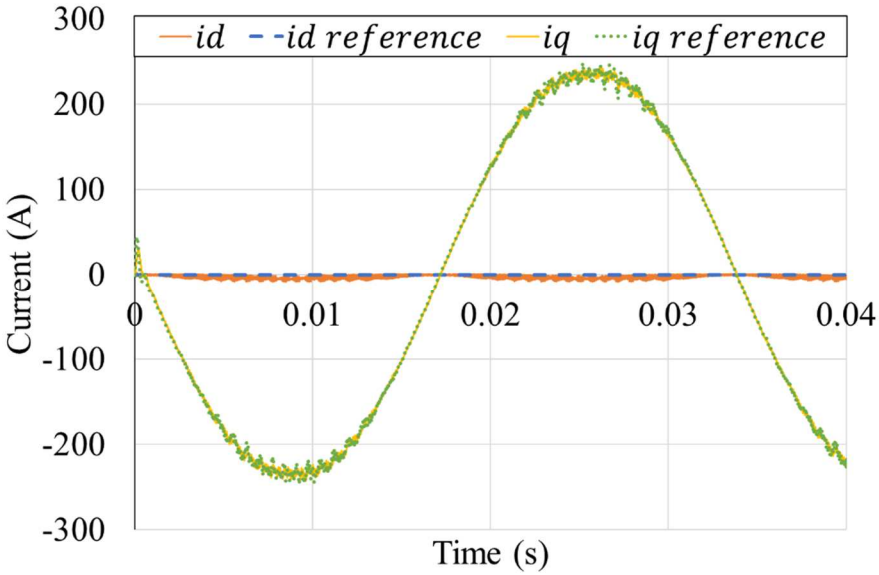

Figure 7: PMLSM controlled currents

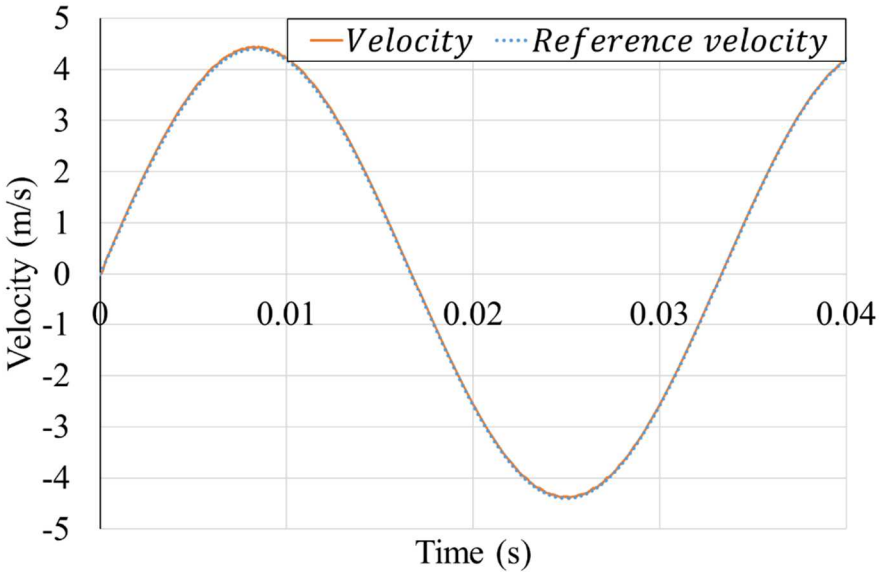

Figure 8: PMLSM controlled velocity

As it is shown in Figure 7 and Figure 8, the system is controlled very well.

5. Combined System Analysis

In order to combine FPSE and PMLSM, it is necessary to link their equations together. From physical point of view, the FPSE power piston is connected to the PMLSM mover as it was

shown in Figure 1. It means that in order to combine these two systems the dynamic equations of the power piston and the mover should be combined. After combination, the equations of the combined system will be as:

$$(m_p + m_m)\ddot{x}_p = A_p P_{mean}\left(\left(1 + \frac{A_p x_p - (A_d - A_{rod})x_d}{T_k V_{avT}} + \frac{A_d x_d}{T_h V_{avT}}\right)^{-1} - \left(\frac{V_B}{V_B - A_p x_p}\right)^{\gamma}\right) + F_{em} - B_v \dot{x}_p \tag{47}$$

$$m_d \ddot{x}_d = A_d \Delta P + A_{rod} P_{mean}\left(\left(1 + \frac{A_p x_p - (A_d - A_{rod})x_d}{T_k V_{avT}} + \frac{A_d x_d}{T_h V_{avT}}\right)^{-1} - \left(\frac{V_D}{V_D - A_{rod} x_d}\right)^{\gamma}\right) \tag{48}$$

$$v_d = L_d \frac{di_d}{dt} + R i_d - \frac{\pi}{\tau}\dot{x}_p L_q i_q \tag{49}$$

$$v_q = L_q \frac{di_q}{dt} + R i_q + \frac{\pi}{\tau}\dot{x}_p \left(L_d i_d + \sqrt{3/2}\,\psi_f\right) \tag{50}$$

$$F_{em} = \frac{\pi}{\tau}\left(\sqrt{3/2}\,\psi_f i_q + (L_d - L_q) i_d i_q\right) \tag{51}$$

$$P_{em} = F_{em}\dot{x}_p \tag{52}$$

$$P_{el} = v_q i_q + v_d i_d \tag{53}$$

Block diagram of the combined system is shown in Figure 9. As it is shown the whole system can be divided into 4 parts: 1- PMLSM model, 2- FPSE model, 3- Inverter and 4- Control system.

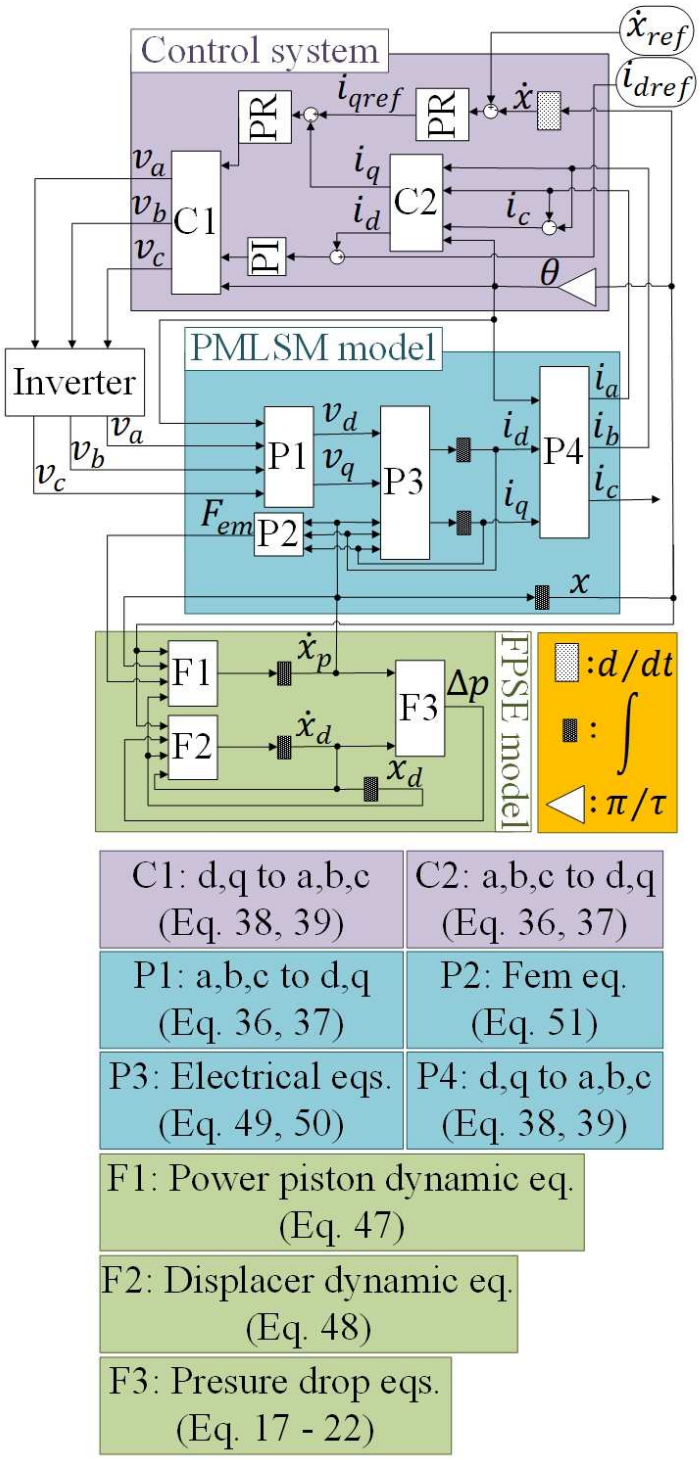

Figure 9: Block diagram of FPSE-PMLSM combined system

The results of the combined system are shown in Figure 10, Figure 11, Figure 12 and Figure 13. The first three figures show the transient behavior and the last one indicates the steady behavior of the system. Input parameters of the combined system are the same parameters of Table 2 and Table 4.

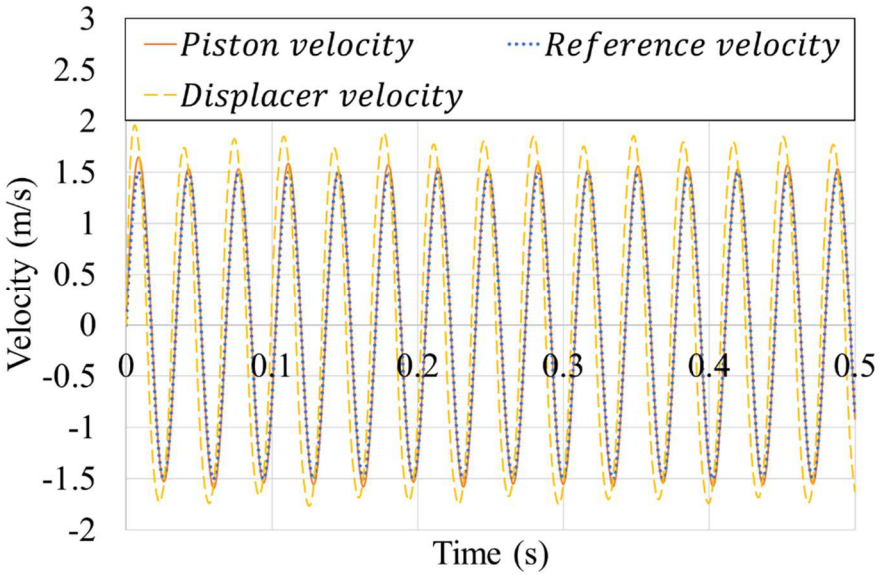

Figure 10: Combined system controlled velocity - Transient

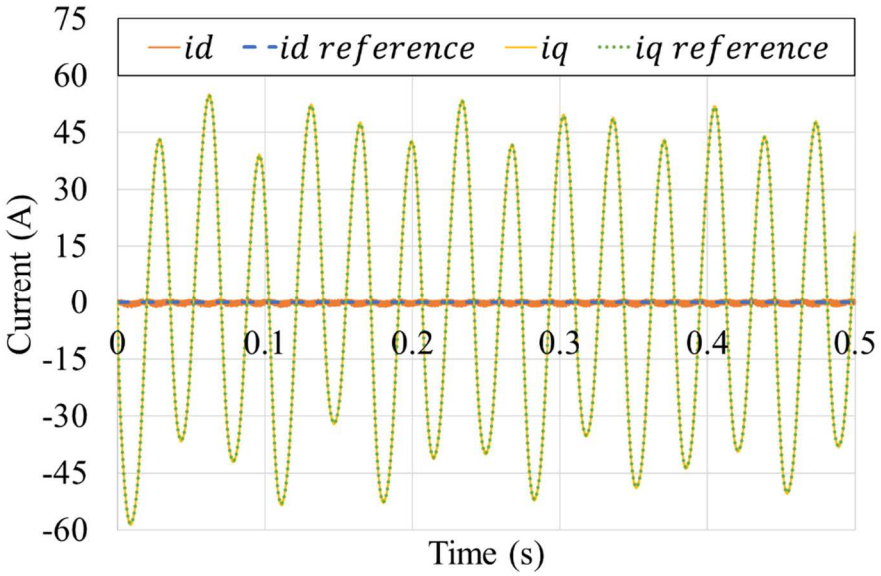

Figure 11: Combined system controlled current - Transient

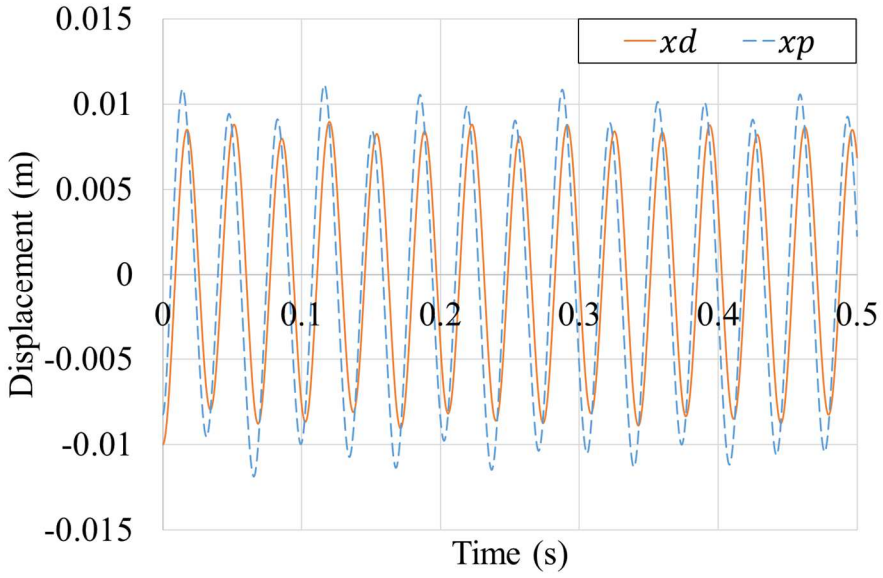

Figure 12: Power & displacer piston displacement in combined system - Transient

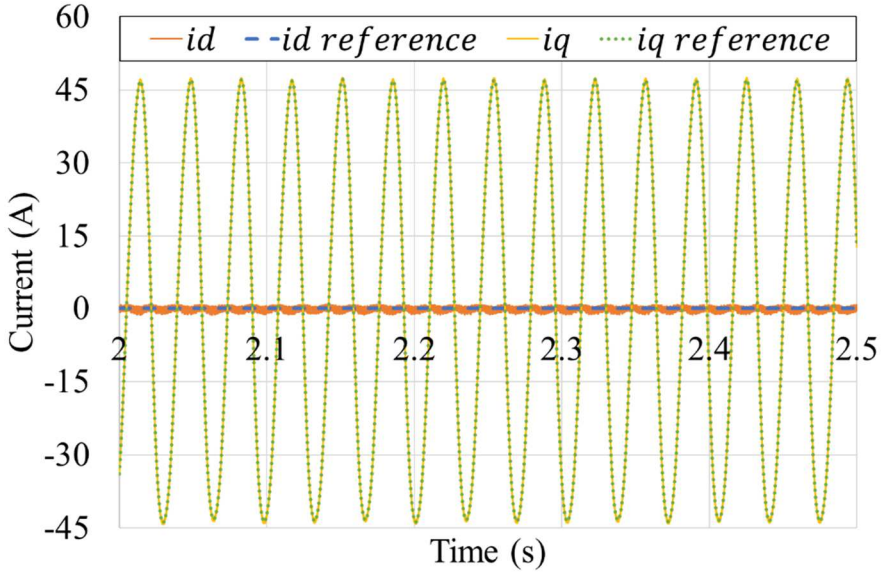

Figure 13 : Combined system controlled current - Steady

Figure 10 shows the power piston and displacer speed variations. As it can be seen in this figure, the piston speed is controlled by using PMLSM speed controller. Also, Figure 11 shows that the PMLSM current is controlled. In Figure 12 the phase shift between power piston and displacer can be seen. Furthermore, Figure 13 identifies the steady behavior of the system that the system will have after a few cycles.

6. Conclusion

The focus of the present study was to analyze a combined system of an FPSE and a PMLSM for this purpose. To study the proposed system, first an accurate model was presented by using nonlinear equations of FPSE for simulation. Other studies simulated this system with linear equations of FPSE. In the present study, by comparing linear and nonlinear models, it was shown that the linear model is not an accurate model for the present case but the nonlinear one is. Thus, a nonlinear model was developed and validated for the FPSE to be used in combined system simulation. Then, PMLSM was modeled and controlled. To combine FPSE with

PMLSM, according to the solid mechanical link between them, their dynamic equations were combined and the results were presented. The control of the system was achieved by controlling the speed and two currents in $d-q$ frame.

By using this accurate combined model, it will be possible to develop new controls of the system in order to reject instabilities coming from heat sources transient behavior. New control methods, can help to improve the performance and efficiency of the system to extract maximum energy of a heat source. In future studies, the experimental setup of the system will also be tested and controlled.

References

[1] R. Stirling, Stirling air engine and the heat regenerator, UK Pat. 4081 (1816).

[2] E. Podesser, Electricity production in rural villages with a biomass Stirling engine, Renew. Energy. 16 (1999) 1049–1052.

[3] B. Kongtragool, S. Wongwises, A review of solar-powered Stirling engines and low temperature differential Stirling engines, Renew. Sustain. Energy Rev. 7 (2003) 131–154.

[4] D.H. Rix, Some aspects of the outline design specification of a 0.5 kW Stirling engine for domestic scale co-generation, Proc. Inst. Mech. Eng. Part A J. Power Energy. 210 (1996) 25–33.

[5] B. Ross, Status of the emerging technology of Stirling machines, IEEE Aerosp. Electron. Syst. Mag. 10 (1995) 34–39.

[6] S.H. Zare, A.R. Tavakolpour-Saleh, Frequency-based design of a free piston Stirling engine using genetic algorithm, Energy. 109 (2016) 466–480.

[7] K. Wang, S.R. Sanders, S. Dubey, F.H. Choo, F. Duan, Stirling cycle engines for recovering low and moderate temperature heat: A review, Renew. Sustain. Energy Rev. 62 (2016) 89–108.

[8] G. Walker, Stirling engines, (1980).

[9] J. Subramanian, G. Heiskell, F. Mahmudzadeh, P. Famouri, Study of radial and axial magnets for linear alternator—Free piston engine system, in: Power Symp. (NAPS), 2017 North Am., IEEE, 2017: pp. 1–6.

[10] R. Redlich, A summary of twenty years experience with linear motors and alternators, Sunpower Inc. (1995).

[11] E.Y. Loktionov, A.A. Martirosyan, M.D. Shcherbina, Solar powered free-piston stirling—Linear alternator module for the lunar base, in: Ind. Eng. Appl. Manuf. (ICIEAM), Int. Conf., IEEE, 2016: pp. 1–6.

[12] J.-M. Kim, J.-Y. Choi, K.-S. Lee, S.-H. Lee, Design and analysis of linear oscillatory single-phase permanent magnet generator for free-piston stirling engine systems, AIP Adv. 7 (2017) 56667.

[13] P. Zheng, B. Yu, S. Zhu, Q. Gong, J. Liu, Research on control strategy of free-piston stirling-engine linear-generator system, in: Electr. Mach. Syst. (ICEMS), 2014 17th Int. Conf., IEEE, 2014: pp. 2300–2304.

[14] T.T. Dang, P. François, L. Prévond, H. Ben Ahmed, Theoretical and experimental results of tubular linear induction generator for Stirling cogenerator system, in: XIX Int. Conf. Electr.

Mach. 2010, IEEE, 2010: pp. 1–7.

[15] T.T. Dang, M. Ruellan, L. Prévond, H. Ben Ahmed, B. Multon, Sizing Optimization of Tubular Linear Induction Generator and Its Possible Application in High Acceleration Free-Piston Stirling Microcogeneration, IEEE Trans. Ind. Appl. 51 (2015) 3716–3733.

[16] T.T. Dang, M. Ruellan, H. Ben Ahmed, L. Prevond, B. Multon, Sizing optimization of tubular linear induction generator for a new stirling micro-cogenerator system, in: Power Electron. Electr. Drives, Autom. Motion (SPEEDAM), 2014 Int. Symp., IEEE, 2014: pp. 1362–1367.

[17] W.P. Hew, J. Jamaludin, M. Tadjuddin, K.M. Nor, Fabrication and testing of linear electric generator for use with a free-piston engine, in: Power Eng. Conf. 2003. PECon 2003. Proceedings. Natl., IEEE, 2003: pp. 277–282.

[18] C.K. Alexander, M.N.O. Sadiku, Fundamentals of Electric Circuits, McGraw-Hill Higher Education, 2007. https://books.google.fr/books?id=SBdigDfQB5cC.

[19] J. Boucher, F. Lanzetta, P. Nika, Optimization of a dual free piston Stirling engine, Appl. Therm. Eng. 27 (2007) 802–811.

[20] H. Karabulut, M. Okur, A.O. Ozdemir, Performance prediction of a Martini type of Stirling engine, Energy Convers. Manag. 179 (2019) 1–12.

[21] P. Zheng, C. Tong, J. Bai, B. Yu, Y. Sui, W. Shi, Electromagnetic design and control strategy of an axially magnetized permanent-magnet linear alternator for free-piston stirling engines, IEEE Trans. Ind. Appl. 48 (2012) 2230–2239.

[22] S. Zhu, G. Yu, O. Jongmin, T. Xu, Z. Wu, W. Dai, E. Luo, Modeling and experimental investigation of a free-piston Stirling engine-based micro-combined heat and power system, Appl. Energy. 226 (2018) 522–533.

[23] I. Urieli, D.M. Berchowitz, Stirling cycle engine analysis, A. Hilger Bristol, 1984.

[24] W.R. Martini, Stirling engine design manual. US Department of Energy, DOE/NASA/3152-78/1, NASA, CR-13518, 1978.

[25] W.M. Kays, A.L. London, Compact heat exchangers, (1984).

[26] G. Remy, Commande optimisée d'un actionneur linéaire synchrone pour un axe de positionnement rapide, (2007).